Hindawi
International Journal of Antennas and Propagation
Volume 2022, Article ID 8207347, 7 pages
https://doi.org/10.1155/2022/8207347

Research Article

Analyses of Grating Lobe and Beam Fixation Problems of Low-Profile Dynamic Antenna

Jibin Liu, Ming Xu, Mingtuan Lin, Yangfei Li, Bowen Deng, Yuanxin Lee, Jihong Zhang, and Peiguo Liu

College of Electronic Science, National University of Defense Technology, Changsha 410073, China

Correspondence should be addressed to Ming Xu; xuming_edu@163.com

Received 15 August 2021; Revised 4 March 2022; Accepted 29 March 2022; Published 15 April 2022

Academic Editor: Paolo Burghignoli

Dynamic metasurface antennas (DMAs) and dynamic antenna arrays (DAAs) are emerging concepts in low-profile antenna design, providing alternative structures with lower circuit complexity and power requirements for radar and communication systems. However, dynamic antennas are prone to significant grating lobe and beam fixation problems due to their discrete amplitude and phase control. The reasons behind these issues are explored through mathematical and simulation analysis of three specific cases, and solutions are subsequently proposed and partially experimentally verified.

1. Introduction

As an emerging alternative to conventional phased antennas, dynamic metasurface antennas have advantages in both cost and manufacturing complexity. This is because expensive phase shifters and transmit/receive (T/R) modules are not required, unlike traditional phased array antennas which are widely applied in security screening [1, 2], satellite communication [3, 4], earth observation [5], etc.

Dynamic metasurface antenna [6–11] beamforming differs from that of phased arrays or electronic scan antennas (ESAs). In traditional antenna arrays, beam scanning can be achieved by configuring all channels in a specific manner and each element is controlled by an independent phase shifter and amplifier. In dynamic antennas, only a single channel is required to achieve beam scanning with each metamaterial element configured by tunable components such as PIN diodes and MEMS switches [12].

Currently, dynamic antennas include reflectarray [13, 14], transmitarray [15–21], and low-profile dynamic antennas. Reflectarray and transmitarray antennas can achieve spatial switching or beam scanning to a certain extent. However, the profiles of both antennas are also higher, which hinders installation. Therefore, demand for low-profile dynamic patch antennas is relatively large.

The integration of the feed source and the metasurface can effectively reduce the overall profile of dynamic antennas and is easy to process and assemble. A low-profile, directly fed, metasurface antenna proposed by Smith et al. uses a waveguide to excite an array of metamaterial radiators [22]. Each metamaterial element radiates energy from the guide wave into free space as it passes through the waveguide. The aperture radiation pattern is the superposition of the radiation of each element. The introduction of separate processable tunable components into each metamaterial element allows radiation patterns to be electronically controlled with guided indicating beams in the available waveforms. However, without active phase shifters and T/R modules, the control of dynamic antenna phase and amplitude is limited, which may cause a large grating lobe under certain conditions [23]. Boyarsky et al. also analysed the grating lobe problem in metasurface antenna arrays [23]. To circumvent this problem, a compensatory waveguide feed layer was introduced, which was designed to suppress grating lobes in metasurface antenna arrays. However, we did not solve this problem through examining the physical

structure, but instead identified a relationship between the grating lobe and the cell spacing through theoretical analysis, circumventing the grating lobe problem by limiting the cell spacing range. A large grating lobe appears at the corresponding negative steering angle in uniform feed DAAs [24]; therefore, in this study, the grating lobes were suppressed using a nonuniform feed. Another problem with DMA is the beam fixation issue, where there is a fixed beam with greater gain, in addition to the steering beam. This paper identified the source of this new problem through theoretical analysis and subsequently solved the issue by limiting the cell spacing.

This paper is arranged as follows. The dynamic antenna grating lobe and beam fixation problems are described in Section 2 via three specific cases. Section 3 proposes solutions for the above problems by theoretical derivation and CST simulation. The solutions are also partially experimentally verified. Finally, the conclusions are drawn in Section 4.

2. Problems of Grating Lobes and Beam Fixation

In this section, simulations of three low-profile dynamic antenna cases are realised using CST software to illustrate the grating lobe and beam fixation problems. The three cases analysed are for low-profile dynamic antennas including dynamic metasurface antennas and dynamic patch antenna arrays.

2.1. Case 1: Grating Lobe Problem of DMA. Currently, DMA can achieve beam scanning, but when the elements are further apart than a certain distance, grating lobe problems can occur. Here, the cELC metasurface antenna proposed by Smith et al. is used to illustrate the grating lobe problem [22]. The antenna consists of a 1-D waveguide with a metamaterial array etched on it. A resonance circuit equivalent to complementary cELCs can generate strong in-plane currents near the resonance point and induce an effective magnetic surface current with a dominant dipole response. The cELC couples to the guided wave transverse magnetic field and radiates as a planar magnetic dipole [25].

In the CST simulation, the spacing between the cELC units is $d = \lambda_0/3$, $\lambda_0 = 10mm$, $\lambda_g = 6.5$mm, and the number of cELC units is $M = 32$. The cELC unit is shown in Figure 1(a). PIN 1 and PIN 2 are in opposite directions. When a DC bias is applied to the cELC centre, the two diodes are in the same state. Therefore, when cELC is in the ON-state (radiation state), it radiates energy outwards. Conversely, in the OFF-state (nonradiation state), cELC does not radiate energy. Each cELC switches between radiation ("1") and nonradiation ("0") states. The effect of element spacing on the DMA dynamic beamforming is illustrated in Figure 1(a), and the steering angle is set to 20° according to the calculation formula in [22]. It can be found that when the distance of the cELC is $\lambda_0/3$, in addition to the main beam at 20°, there is also a large grating lobe at −37°. The problem of grating lobes for larger unit spacing still needs to be resolved.

2.2. Case 2: Grating Lobe Problem of DAA. Similarly, the grating lobe problem also exists for DAA composed of patch antenna units. Here, the 1-D dynamic patch antenna array [24] with uniform feed proposed in our previous work is used to demonstrate the grating lobe problem, as shown in Figure 1(b). The proposed antenna element configuration consists of two patches, a feeder network, a ground plane, and two-layer dielectrics. Patch 1 and patch 2 are printed symmetrically on the left and right sides, and the two PIN diodes have the same direction. The two patches work separately controlled by the two PIN diodes to achieve a 180° phase difference and mimic the two basic digital elements "−1" and "1."

In the CST simulation, the spacing between the antenna units is $d = \lambda_0/2$, the operating frequency is 9 GHz, and the number of antenna units is $M = 32$. The antenna pattern with a uniform feed and a steering angle of 20° is shown in Figure 1(b), where it can be seen that there is a main beam at 20° and a large grating lobe at −20°. In the following analysis, the grating lobes are suppressed by nonuniform feeding.

2.3. Case 3: Beam Fixation Problem of DMA. In addition to the grating lobe problem, there is also the problem of beam fixation with DMA. Theoretically, DMA should have good pointing beams for any steering angles and different coding. However, when the element spacing d satisfies a particular condition, the beam direction remains unchanged regardless of the antenna encoding state. Taking the antenna of Case 1 as an example, when the beam scanning angle is set from −10° to −30°, there is always a fixed beam of −25° with a higher gain than the steering angle, as shown in Figure 1(c), which affects the antenna performance.

3. Analyses of Grating Lobes and Beam Fixation

This section firstly theoretically analyses the large grating lobe and beam fixation problems of low-profile dynamic antennas and then proposes corresponding solutions. Finally, conclusions are partially verified experimentally.

The following general behaviour mode was used to cover low-profile antennas (DMA and DAA):

$$\begin{cases} F(\psi = 2n\pi) & = 1, n = 1, 2 \ldots \text{(main beam)}, \\ \psi & = \xi + \text{kd} \sin\theta, \end{cases} \tag{1}$$

where F is the normalized gain, ξ is the excitation phase, $k\,d\,\sin\,\theta$ is the propagation phase, n is an integer, d is the spacing between any two adjacent elements, k_g is the complex propagation constant of the waveguide, k is the free-space propagation constant, and θ is the steering angle. For DMA, $\xi = k_g d$. For DAA with a uniform feed, $\xi = 0$ or a constant. For a nonuniform feed, $\xi = \{\Phi_m\}$. In order to show the problems more clearly, we analysed the two low-profile antennas in three cases based on the above-mentioned general behaviour mode.

3.1. Analyses of Case 1 (Grating Lobe Problem of DMA). The grating lobe problem results in an unplanned angle θ_1 occurring outside the steering angle θ_0. As shown in

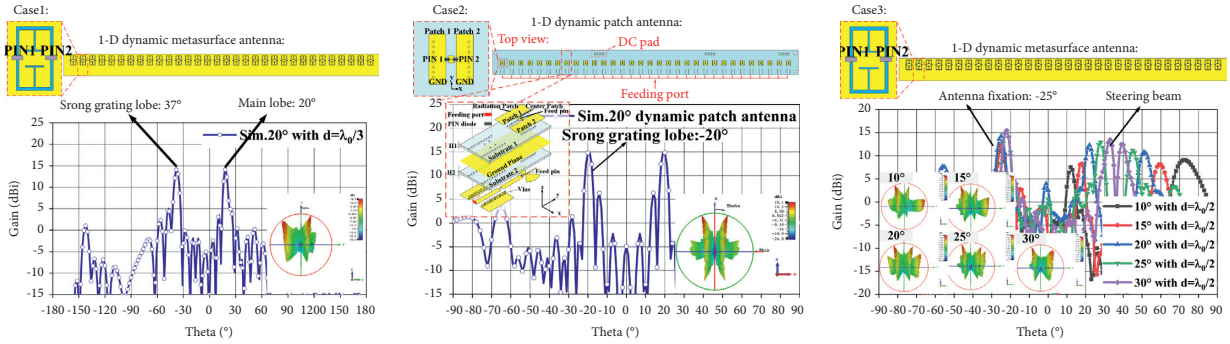

FIGURE 1: The grating lobe and beam fixation problems simulated by CST. (a) Grating lobe problem for the dynamic metasurface antenna (where $M = 32$; $\lambda_0 = 10$mm; and $\lambda_g = 6.5$mm). (b) Grating lobe problem for the dynamic patch antenna (where $M = 32$ and element spacing $d = \lambda_0/2$). (c) Beam fixation problem for dynamic metasurface antennas (where $M = 32$; $\lambda_0 = 10$mm; and $\lambda_g = 6.5$mm).

Figure 2, when the main beams are steered at θ_0, the following formula can be obtained for the waveguide-based dynamic metasurface antenna:

$$\left(k_g - k_0 \sin\,\theta_0\right)d = 2m_0\pi, \tag{2}$$

where k_g is the complex propagation constant of the waveguide, k_0 is the free-space propagation constant, θ_0 is the steering angle, d is the distance between the antenna elements, and m_0 and m_1 are integers. Similarly, the grating lobe θ_1 should also satisfy

$$\left(k_g - k_0 \sin\,\theta_1\right)d = 2m_1\pi. \tag{3}$$

For $\theta_0 \neq \theta_1$, the following formulation can be deduced from (3):

$$\left(k_g - k_0 \sin\,\theta_0\right)d + \left(k_g - k_0 \sin\,\theta_1\right)d = 2\left(m_0 + m_1\right)\pi = 2m\pi. \tag{4}$$

Generally, setting $m = 1$:

$$\left(2k_g - k_0\left(\sin\,\theta_0 + \sin\,\theta_1\right)\right)d = 2\pi, \tag{5}$$

$$-1 \leq \sin\,\theta_1 = 2\frac{\lambda_0}{\lambda_g} - \frac{\lambda_0}{d} - \sin\,\theta_0 \leq 1, \tag{6}$$

where λ_g is the waveguide wavelength and λ_0 is the free-space wavelength. The mathematical relationship between the main lobe and the grating lobe can be obtained from (6). When the main lobe is 20°, the grating lobe can be calculated as −36.7° through (6), which is consistent with the simulation result in Figure 1(a). From (6), the following formulation can be derived:

$$\frac{\lambda_0}{\left(2\lambda_0/\lambda_g - \sin\,\theta_0 + 1\right)} \leq d \leq \frac{\lambda_0}{\left(2\lambda_0/\lambda_g - \sin\,\theta_0 - 1\right)}. \tag{7}$$

The constraint of (7) on the cell spacing must be removed to eliminate the grating lobes. Therefore, it can be derived from (7):

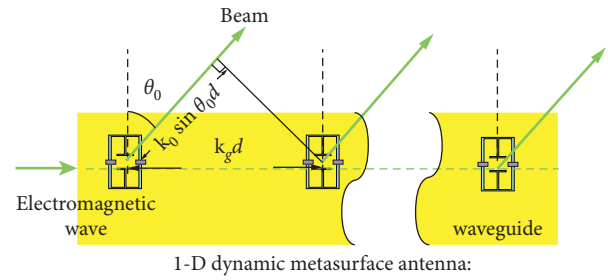

FIGURE 2: Schematic diagram of beam scanning of DMA.

$$\begin{cases} d > \dfrac{\lambda_0}{\left(2\lambda_0/\lambda_g - \sin\,\theta_0 - 1\right)}, \\ d < \dfrac{\lambda_0}{\left(2\lambda_0/\lambda_g - \sin\,\theta_0 + 1\right)}. \end{cases} \tag{8}$$

Avoiding grating lobes at any angle θ_0 can be derived from (88):

$$d > \frac{\lambda_0}{2\lambda_0/\lambda_g - 2}, \tag{9}$$

or

$$d < \frac{\lambda_0}{\left(2\lambda_0/\lambda_g + 2\right)}. \tag{10}$$

If (9) and (10) are satisfied, the grating lobe problem can theoretically be avoided. However, from Case 3 analysis, a beam fixation problem also appears when the elements are further apart than a certain distance. Consequently, condition (10) is more appropriate. To gain a more intuitive understanding (10), this conclusion is simulated in CST. In the CST simulation, $\lambda_0 = 10$ mm, $\lambda_g = 6.5$ mm, and the number of antenna units is $M = 32$. It is worth noting that the size of the cELC unit is $1.2\,\text{mm} \times 1.9\,\text{mm}$ $(0.12\lambda_0 \times 0.19\lambda_0)$. Therefore, the cell spacing d should be greater than $0.12\lambda_0$. On the other hand, d must satisfy

$d < \lambda_0/(2\lambda_0/\lambda_g + 2) = 1.97\text{mm} = \lambda_0/5$; otherwise, large grating lobes will appear. As shown in Figure 3(a), when the element spacing d satisfies this condition ($d = 0.15\lambda_0$, $0.16\lambda_0$, $0.17\lambda_0$, and $0.19\lambda_0$), no large grating lobes are formed beyond a 25° steering angle. In fact, the antenna works within a specific steering angle range, such as $-45^\circ \sim 45^\circ$. Therefore, not all steering angles need to satisfy (8). When the steering angle $\theta_0 = 45^\circ$, from (8), it can be deduced that $d < 0.29\lambda_0$, and therefore the grating lobe problem is avoided, as shown in Figure 4. However, when the steering angle is greater than 45°, grating lobe problems may appear.

3.2. Analyses of Case 2 (Grating Lobe Problem of DAA). Similarly, DAA also experiences a grating lobe problem. From the simulation results in Figure 1(b), uniform feeding is the source of the grating lobe problem with DAA. Here, the origin of this phenomenon is derived mathematically and the problem is solved by introducing a nonuniform feed.

For a 1-bit dynamic patch antenna, its far-field radiation diagram is as follows:

$$F(\phi,\theta) = \sum_{m=1}^{M} f_m(\phi,\theta) e^{\left(jm2\pi/\lambda d \sin\ \theta - \varphi_m\right)}, \tag{11}$$

where d is the distance between adjacent antenna elements, M is the total number of elements, θ is the steering angle, and φ is the azimuth angle. The current antenna element direction graph is $f_m(\phi,\theta)$, and φ_m refers to the two states of the antenna element (namely, 0 or π).

According to the above formula, the patch antenna coding principle is mainly to synthesize the required phase in each radiator position; then, sample the phase distribution to two states. φ_m can be written according to the following formula:

$$\varphi_m = j^* \text{round}\left(\frac{\cos\left(2\pi/\lambda \text{md} \sin\ \theta_0 + \Phi_m\right) + 1}{2}\right) * \pi, \tag{12}$$

where θ_0 is the steering angle and Φ_m is the reference phase of the mth port.

For uniform feeding, $\Phi_m = {}^{0^\circ}$ or a constant. According to (12), it can be found that $-\theta_0$ and θ_0 can both satisfy (12) for uniform feeding. Hence, a large grating lobe will be generated at $-\theta_0$. To avoid this phenomenon, a disturbance factor is added to the excitation phase of each element. Here, we use a nonuniform feed to excite the array, where Φ_m is no longer a fixed constant. At this time, $\{\Phi_m\}$ breaks the symmetry of (12).

The nonuniform feed proposed in this article is essentially different from the random phase proposed by Smith et al. Firstly, the random phase, as a disturbance factor, is added to the decision criterion, which breaks the phase symmetry of (11), but it does not change the feeding network. However, a nonuniform feed is a physical component such as a transmission line network or coaxial cable feeding network with unequal length, which can be incarnated into the phase value $\{\Phi_m\}$. In addition, the random phase solves the sidelobe problem, while the nonuniform feeding solves the grating lobe problem. It is noted that the random phase can also be introduced to further suppress sidelobes for nonuniformly fed DAA.

The comparison of simulated antenna patterns of the antenna array, with and without nonuniform feed, at 10°, is shown in Figure 3(b). When the nonuniform feed is introduced, no large grating lobe is formed at the corresponding negative angle, which confirms that introducing a nonuniform feed is effective in suppressing the strong grating lobe.

3.3. Analyses of Case 3 (Beam Fixation Problem of DMA). Beam fixation means that no matter what the encoding, there is always a fixed angle θ whose gain is greater than the steering angle θ_0. Consequently, there is always a fixed angle θ for waveguide-fed DMA which satisfies

$$k_g d = k_0 d \sin\ \theta + 2m\pi, \tag{13}$$

$$\text{then} \quad -1 \le \sin\ \theta = \lambda_0\left(\frac{1}{\lambda_g} - \frac{m}{d}\right) \le 1. \tag{14}$$

For most cases, $\lambda_g < \lambda_0$. Therefore, it can be derived from (14):

$$\frac{m\lambda_0\lambda_g}{\lambda_0 + \lambda_g} \le d \le \frac{m\lambda_0\lambda_g}{\lambda_0 - \lambda_g}, \lambda_g < \lambda_0. \tag{15}$$

To prevent the beam fixation problem, restriction (15) must be removed. In practice, we generally set $m = 1$, and the beam control conclusions can be drawn as follows:

$$d < \frac{\lambda_0\lambda_g}{\lambda_0 + \lambda_g}. \tag{16}$$

To validate this conclusion, the same model as Case 1 is used for analysis. From (15), when the element spacing $d < \lambda_0\lambda_g/\lambda_0 + \lambda_g = 2\lambda_0/5$, the beam fixation problem does not occur. As shown in Figure 3(c), when the element spacing $d = \lambda_0/5$, the beam steers normally.

3.4. Measurement Result. In our previous work [24], we fabricated a 1-D dynamic array antenna which can be directly used to verify the solution of Case 2. Cases 1 and 3 can also be validated experimentally. However, only Case 2 is verified here due to the length limitation of the paper and for simplicity. Figure 5 shows images of the measurement setup in an anechoic chamber. The 1-D array antenna is fixed on the turntable in the microwave anechoic chamber, and a standard gain horn is used as the transmitting antenna for the pattern measurement. Uniform feeding adopts a 32-way power divider to connect with 32 units of the array antenna, through 32 equal length coaxial cables. Conversely, nonuniform feeding uses unequal length coaxial cables. The corresponding phase values of the unequal length cables are displayed in Figure 5. The comparison of the antenna array measured antenna patterns, with and without nonuniform feed at 10°, is also shown in Figure 5. When using a uniform feed, it is found that the gain at −10° grating lobe is lower than 10° steering angle. This is due to the unequal length of

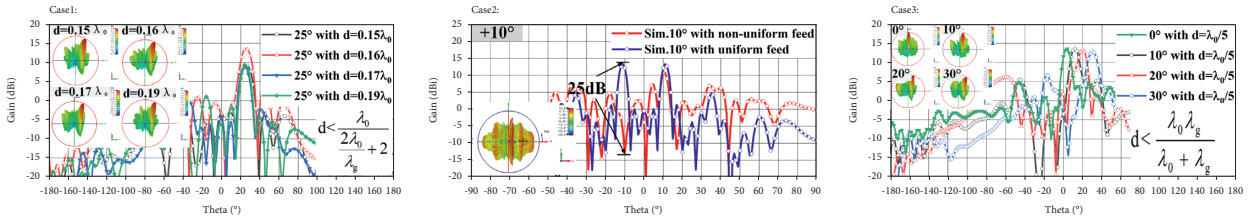

Figure 3: The solution of grating lobes and beam fixation simulated by CST. (a) Antenna patterns of different element spacings d (where $m = 1$; $\lambda_0 = 10$mm; and $\lambda_g = 6.5$mm) for dynamic metasurface antenna. (b) Antenna patterns of dynamic patch antenna with nonuniform feed in CST. (c) The simulated scanning beam pattern when element spacing d is $\lambda_0/5$.

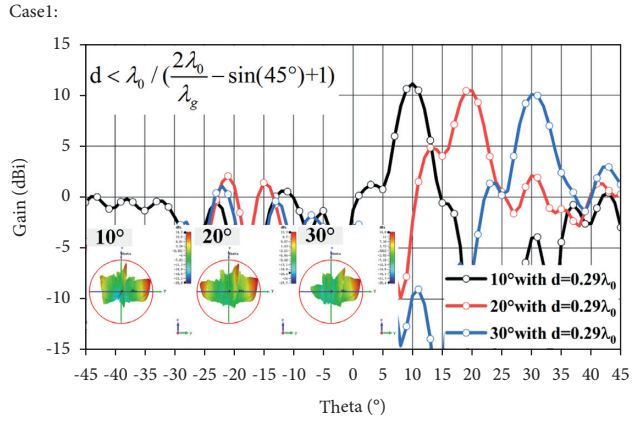

Figure 4: Antenna pattern of DMA with $d = 0.29\lambda_0$.

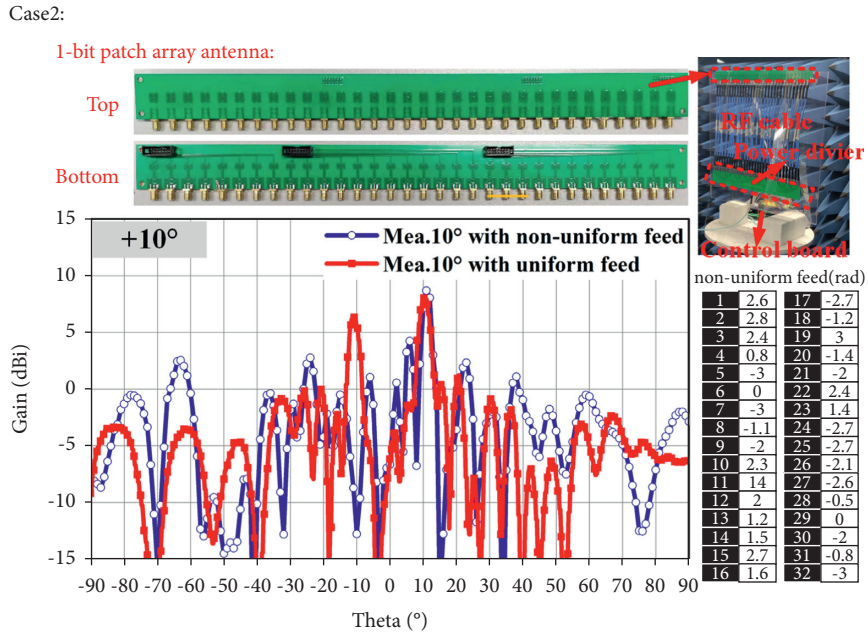

Figure 5: Comparison of measured scanning beam pattern with and without nonuniform feed of the 1-D patch array at 10°.

the cables. However, the difference between the cables is minimal, resulting in a smaller gain reduction. When using a nonuniform feed, the gain is greatly reduced at −10° compared with a uniform feed. The measurement results are in good agreement with the simulation, indicating that the nonuniform feed effectively suppresses the grating lobes.

4. Conclusion

To solve both the grating lobe and beam fixation problems in low-profile dynamic antennas, the causes are theoretically revealed using CST simulations. The solutions are proposed based on the results and partially verified. These analyses can help extensively promote the engineering application of dynamic antennas.

Data Availability

The data used to support the findings of this study are available from the corresponding author upon request.

Conflicts of Interest

The authors declare that they have no conflicts of interest.

Acknowledgments

This study was supported in part by the National Natural Science Foundation of China under grant no. 61901491 and in part by the National Natural Science Foundation of Hunan Province under grant no. 2020JJ5665.

References

[1] Michael, T. Boyarsky, Sleasman et al., "Synthetic aperture radar with dynamic metasurface antennas: a conceptual development," *Journal of the Optical Society of America*, vol. 34, pp. 22–36, 2017.

[2] J. Hunt, T. Driscoll, A. Mrozack et al., "Metamaterial apertures for computational imaging," *Science*, vol. 339, no. 6117, pp. 310–313, 2013.

[3] J. N. Gollub, O. Yurduseven, K. P. Trofatter et al., "Large metasurface aperture for millimeter wave computational imaging at the human-scale," *Scientific Reports*, vol. 7, no. 1, Article ID 42650, 2017.

[4] M. C Johnson, B Mikala, K. Brunton, K. Kundtz, and J. N. Kutz, Sidelobe canceling for reconfigurable holographic metamaterial antenna," *IEEE Transactions on Antennas and Propagation*, vol. 63, no. 4, pp. 1881–1886, 2015.

[5] R. Stevenson, M. Sazegar, A. Bily, M. Johnson, and N. Kundtz, "Metamaterial surface antenna technology: commercialization through diffractive metamaterials and liquid crystal display manufacturing," in *Proceedings of the 2016 10th International Congress on Advanced Electromagnetic Materials in Microwaves and Optics (METAMATERIALS)*, pp. 349–351, Chania, Greece, September 2016.

[6] C. Pfeiffer and A. Grbic, "Metamaterial huygens' surfaces: tailoring wave fronts with rs," *Physical Review Letters*, vol. 110, no. 19, Article ID 197401, 2013.

[7] J. P. S. Wong, M. Selvanayagam, and G. V. Eleftheriades, "Design of unit cells and demonstration of methods for synthesizing huygens metasurfaces," *Photonics and Nanostructures - Fundamentals and Applications*, vol. 12, no. 4, pp. 360–375, 2014.

[8] C. Pfeiffer and A. Grbic, "Cascaded metasurfaces for complete phase and polarization control," *Applied Physics Letters*, vol. 102, no. 23, Article ID 231116, 2013.

[9] Y. Zhao, N. Engheta, and A. Alù, "Homogenization of plasmonic metasurfaces modeled as transmission-line loads," *Metamaterials*, vol. 5, no. 2-3, 2011.

[10] D. Sievenpiper, J. Schaffner, R. Loo, G. Tangonan, S. Ontiveros, and R. Harold, "A tunable impedance surface performing as a reconfigurable beam steering reflector," *IEEE Transactions on Antennas and Propagation*, vol. 50, no. 3, pp. 384–390, 2002.

[11] D. F. Sievenpiper, J. H. Schaffner, H. J. Song, R. Y. Loo, and G. Tangonan, "Two-dimensional beam steering using an electrically tunable impedance surface," *IEEE Transactions on Antennas and Propagation*, vol. 51, no. 10, pp. 2713–2722, 2003.

[12] T. Sleasman, M. F. Imani, W. Xu et al., "Waveguide-fed tunable metamaterial element for dynamic apertures," *IEEE Antennas and Wireless Propagation Letters*, vol. 15, pp. 606–609, 2016.

[13] O. Bayraktar, O. A. Civi, and T. Akin, "Beam switching reflectarray monolithically integrated with rf mems switches," *IEEE Transactions on Antennas and Propagation*, vol. 60, no. 2, pp. 854–862, 2012.

[14] M. Lin, "Single sensor to estimate doa with programmable metasurface," *IEEE Internet of Things Journal*, vol. 99, 2021.

[15] R. Zhang and R. Ma, "A novel 24ghz lens antenna based on phase gradient metasurface," in *Proceedings of the 2019 Cross Strait Quad-Regional Radio Science and Wireless Technology Conference*, July 2019.

[16] C. G. M. Ryan, M. R. Chaharmir, J. Shaker, J. R. Bray, Y. M. M. Antar, and A. Ittipiboon, "A wideband transmitarray using dual-resonant double square rings," *IEEE Transactions on Antennas and Propagation*, vol. 58, no. 5, pp. 1486–1493, 2010.

[17] M. A. Al-Joumayly and N. Behdad, "Wideband planar microwave lenses using sub-wavelength spatial phase shifters," *IEEE Transactions on Antennas and Propagation*, vol. 59, no. 12, pp. 4542–4552, 2011.

[18] C. C. Chih-Chieh Cheng, B. Lakshminarayanan, and A. Abbaspour-Tamijani, "A programmable lens-array antenna with monolithically integrated mems switches," *IEEE Transactions on Microwave Theory and Techniques*, vol. 57, no. 8, pp. 1874–1884, 2009.

[19] P. Padilla, A. Muñoz-Acevedo, M. Sierra-Castañer, and M. Sierra-Pérez, "Electronically reconfigurable transmitarray at ku band for microwave applications," *IEEE Transactions on Antennas and Propagation*, vol. 58, no. 8, pp. 2571–2579, 2010.

[20] M. Li and N. Behdad, "Ultra-wideband, true-time-delay, metamaterial-based microwave lenses," in *Proceedings of the 2012 IEEE International Symposium on Antennas and Propagation*, pp. 1-2, Chicago, IL, USA, July 2012.

[21] S. Kamada, N. Michishita, and Y. Yamada, "Metamaterial Lens Antenna Using Dielectric Resonators for Wide Angle Beam Scanning," in *Proceedings of the 2010 IEEE Antennas and Propagation Society International Symposium*, pp. 1–4, Toronto, ON, Canada, July 2010.

[22] D. R. Smith, O. Yurduseven, L. P. Mancera, P. Bowen, and N. B. Kundtz, "Analysis of a waveguide-fed metasurface

antenna," *Phys.rev.applied*, vol. 8, no. 5, Article ID 054048, 2017.

[23] M. Boyarsky, M. F. Imani, and D. R. Smith, "Grating lobe suppression in metasurface antenna arrays with a waveguide feed layer," *Optics Express*, vol. 28, no. 16, pp. 23991–24004, 2020.

[24] S. Pan, M. Xu, S. Zhu, M. Lin, and G. Li, "A low-profile programmable beam scanning array antenna," in *Proceedings of the 2021 International Conference on Microwave and Millimeter Wave Technology (ICMMT)*, pp. 1–3, Nanjing, China, May 2021.

[25] N. Landy, J. Hunt, and D. R. Smith, "Homogenization analysis of complementary waveguide metamaterials," *Photonics and Nanostructures - Fundamentals and Applications*, vol. 11, no. 4, pp. 453–467, 2013.